Research Article | Vol. 26, No. 5 | 5 Mar 2018 | OPTICS EXPRESS 5724
Optics EXPRESS

Experimental characterization of continuous-variable orbital angular momentum entanglement using Stokes-operator basis

CHUNXIAO CAI,[1,2] LONG MA,[1,2] JUAN LI,[1,2] HUI GUO,[1,2] KUI LIU,[1,2,*] HENGXIN SUN,[1,2] AND JIANGRUI GAO[1,2]

[1] *State Key Laboratory of Quantum Optics and Quantum Optics Devices, Institute of Opto-Electronics, Shanxi University, Taiyuan, Shanxi 030006, China*
[2] *Collaborative Innovation Center of Extreme Optics, Shanxi University, Taiyuan, Shanxi 030006, China*
[*] *liukui@sxu.edu.cn*

Abstract: The continuous-variable (CV) orbital angular momentum (OAM) entanglement is very different to the traditional quadrature entanglement. The Stokes-operators directly reflect the character of OAM light. Here, we report the first direct experimental demonstration the Stokes-operator entanglement of continuous-variable OAM entanglement. Generated by transforming quadrature entanglement in the HG_{01} mode onto the orbital Stokes-operator basis, the entanglement is measured in the Stokes-operator basis using a self-designed detection scheme. An inseparability of $I(\hat{O}_2, \hat{O}_3) < 1$ is achieved over a wide analyzing frequency of 1–10 MHz. Moreover, experimental fluctuations at 5.0 MHz are visualized using the quantum orbital Poincaré sphere representation. The OAM entanglement with Stokes-operators measurement has a promising application in certain nonlocal quantum information protocols and rotational optomechanics by interacting with nanoparticle or atoms.

OCIS codes: (270.0270) Quantum optics; (190.4410) Nonlinear optics, parametric processes; (270.5585) Quantum information and processing.

References and links

1. N. Korolkova, G. Leuchs, R. Loudon, T. C. Ralph, and C. Silberhorn, "Polarization squeezing and continous-variable polarization entanglement," Phys. Rev. A **65**(2), 052306 (2002).
2. L. Allen, M. W. Beijersbergen, R. J. C. Spreeuw, and J. P. Woerdman, "Orbital angular-momentum of light and the transformation of Laguerre–Gaussian laser modes," Phys. Rev. A **45**, 8185–8189 (1992).
3. X. L. Wang, X. D. Cai, Z. E. Su, M. C. Chen, D. Wu, L. Li, N. L. Liu, C. Y. Lu, and J. W. Pan, "Quantum teleportation of multiple degrees of freedom of a single photon," Nature **518**, 516–519 (2015).
4. N. Bozinovic, Y. Yue, Y. Ren, M. Tur, P. Kristensen, H. Huang, A. E. Willner, and S. Ramachandran, "Terabit-scale orbital angular momentum mode division multiplexing in fibers" Science **340**, 1545 (2013).
5. M. P. J. Lavery, Ch. Peuntinger, K. Günthner, P. Banzer, D. Elser, R. W. Boyd, M. J. Padgett, Ch. Marquardt, and G. Leuchs, "Free-space propagation of high-dimensional structured optical fields in an urban environment," Sci. Adv. **3**, 1700552 (2017).
6. J. Wang, J. Y. Yang, I. M. Fazal, N. Ahmed, Y. Yan, H. Huang, Y. X. Ren, Y. Yue, S. Dolinar, M. Tur, and A. E. Willner, "Terabit free-space data transmission employing orbital angular momentum multiplexing," Nat. Photonics **6**, 488–496 (2012).
7. A. E. Willner, H. Huang, Y. Yan, Y. Ren, N. Ahmed, G. Xie, C. Bao, L. Li, Y. Cao, Z. Zhao, J. Wang, M. P. J. Lavery, M. Tur, S. Ramachandran, A. F. Molisch, N. Ashrafi, and S. Ashrafi, "Optical communications using orbital angular momentum beams," Adv. Opt. Photon. **7**(1), 66–106 (2015).
8. A Nicolas, L Veissier, L Giner, E Giacobino, D Maxein, and J Laurat, "A quantum memory for orbital angular momentum photonic qubits," Nat. Photonics **8**, 234–238 (2014).
9. A. Sit, F. Bouchard, R. Fickler, J. Gagnon-Bischoff, H. Larocque, K. Heshami, D. Elser, C. Peuntinger, K. Günthner, B. Heim, C. Marquardt, G. Leuchs, R. W. Boyd, and E. Karimi, "High-dimensional intracity quantum cryptography with structured photons," Optica **4**(9), 1006–1010 (2017).
10. V. D'Ambrosio, N. Spagnolo, L. Del Re, S. Slussarenko, Y. Li, L. C. Kwek, L. Marrucci, S. P. Walborn, L. Aolita, and F. Sciarrino, "Photonic polarization gears for ultra-sensitive angular measurements," Nat. Commun. **4**, 2432 (2013).
11. R. Fickler, R. Lapkiewicz, W. N. Plick, M. Krenn, C. Schaeff, S. Ramelow, and A. Zeilinger, "Quantum entanglement of high angular momenta," Science **338**(6107), 640–643 (2012).

#317951 https://doi.org/10.1364/OE.26.005724
Journal © 2018 Received 19 Dec 2017; revised 14 Feb 2018; accepted 15 Feb 2018; published 26 Feb 2018

Optics EXPRESS

12. C. Cai, K. Liu, and J. Gao, "Rotation angular measurement beyond quantum noise limit with an orbital angular position squeezed state," in Quantum Information and Measurement (Optical Society of America, 2017), pp. QF3A-5.
13. N. K. Langford, R. B. Dalton, M. D. Harvey, J. L. O'Brien, G. J. Pryde, A. Gilchrist, S. D. Bartlett, and A. G. White, "Measuring entangled qutrits and their use for quantum bit commitment," Phys. Rev. Lett. **93**, 053601 (2004).
14. A. Mair, A. Vaziri, G. Weihs, and A. Zeilinger, "Entanglement of the orbital angular momentum states of photons," Nature **412**, 313–316 (2001).
15. A. M. Yao, and M. J. Padgett, "Orbital angular momentum: origins, behavior and applications," Adv. Opt. Photon. **3**, 161–204 (2011).
16. M. Krenn, M. Huber, R. Fickler, R. Lapkiewicz, S. Ramelow, and A. Zeilinger, "Generation and confirmation of a (100 x 100)-dimensional entangled quantum system," Proc. Natl. Acad. Sci. USA **111**, 6243–6247 (2014).
17. G. Molina-Terriza, J. P. Torres, and L. Torner, "Twisted photons," Nat. Phys. **3**, 305–310 (2007).
18. R. Fickler, G. Campbell, B. Buchler, P. K. Lam, and A. Zeilinger, "Quantum entanglement of angular momentum states with quantum numbers up to 10,010," PNAS **113**(48), 13642–13647 (2016).
19. M. Malik, M. Erhard, M. Huber, M. Krenn, R. Fickler, and A. Zeilinger, "Multi-photon entanglement in high dimensions," Nat. Photonics **10**(4), 248–252 (2016).
20. M. Erhard, R. Fickler, M. Krenn, A. Zeilinger, "Twisted photons: new quantum perspectives in high dimensions," https://arXiv:1708.06101 (2017).
21. M. J. Padgett, "Orbital angular momentum 25 years on," Opt. Express **25**(10), 11265–11274 (2017).
22. M. T. L. Hsu, W. P. Bowen, and P. K. Lam, "Spatial-state stokes-operator squeezing and entanglement for optical beams," Phys. Rev. A **79**, 043825 (2009).
23. M. Lassen, G. Leuchs, and U. L. Andersen, "Continuous variable entanglement and squeezing of orbital angular momentum states," Phys. Rev. Lett. **102**, 163602 (2009).
24. B. dos Santos, K. Dechoum, and A. Khoury, "Continuous-variable hyperentanglement in a parametric oscillator with orbital angular momentum," Phys. Rev. Lett. **103**, 230503 (2009).
25. K. Liu, J. Guo, C. Cai, S. Guo, and J. Gao, "Experimental generation of continuous-variable hyperentanglement in an optical parametric oscillator," Phys. Rev. Lett. **113**, 170501 (2014).
26. H. Shi and M. Bhattacharya, "Optomechanics based on angular momentum exchange between light and matter," J. Phys. B **49**, 153001 (2015).
27. N. Behbood, F. Martin Ciurana, G. Colangelo, M. Napolitano, G. Tóth, R. J. Sewell, and M. W. Mitchell, "Generation of macroscopic singlet states in a cold atomic ensemble," Phys. Rev. Lett. **113**, 093601 (2014).
28. C. Peuntinger, B. Heim, C. R. Müller, C. Gabriel, Ch. Marquardt, and G. Leuchs, "Distribution of squeezed states through an atmospheric channel," Phys. Rev. Lett. **113**, 060502 (2014).
29. D. Elser, T. Bartley, B. Heim, C. Wittmann, D. Sych and G. Leuchs, "Feasibility of free space quantum key distribution with coherent polarization states," New J. Phys. **11**(4), 045014 (2009).
30. J. Guo, C. Cai, L. Ma, K. Liu, H. Sun, and J. Gao, "Measurement of Stokes-operator squeezing for continuous-variable orbital angular momentum," Sci. Rep. **7**, 4434 (2017).
31. W. P. Bowen, N. Treps, R. Schnabel, and P. K. Lam, "Experimental demonstration of continuous variable polarization entanglement," Phys. Rev. Lett **89**, 253601 (2002).
32. M. Padgett and J. Courtial, "Poincaré-sphere equivalent for light beams containing orbital angular momentum," Opt. Lett. **24**, 430–432 (1999).
33. J. Guo, C. Cai, L. Ma, K. Liu, H. Sun, and J. Gao, "Higher order mode entanglement in a type ii optical parametric oscillator," Opt. Express **25**, 4985–4993 (2017).
34. M. Lassen, V. Delaubert, C. C. Harb, P. K. Lam, N. Treps, and H. A. Bachor, "Generation of squeezing in higher order Hermite–Gaussian modes with an optical parametric amplifier," J. Eur. Opt. Soc. Rapid Publ. **1**, 06003 (2006).
35. J. T. Barreiro, T. C. Wei, and P. G. Kwiat, "Beating the channel capacity limit for linear photonic superdense coding," Nat. Phys. **4**, 282 (2008).
36. L. Kong, R. Liu, Z. Wang, Y. Si, W. Qi, S. Huang, C. Tu, Y. Li, W. Hu, F. Xu, Y. Lu, and H. Wang, "Complete orbital angular momentum Bell-state measurement and superdense coding," https://arXiv:1709.03770 (2017).
37. M. Lassen, V. Delaubert, J. Janousek, K. Wagner, H. A. Bachor, P. Lam, N. Treps, P. Buchhave, C. Fabre, and C. Harb, "Tools for multimode quantum information: modulation, detection, and spatial quantum correlations," Phys. Rev. Lett. **98**, 083602 (2007).
38. Z. Yin and T. Li,"Bringing quantum mechanics to life: from Schrödinger's cat to Schrödinger's microbe," Contemp. Phys. **58**(2), 119–139 (2017).

1. Introduction

Light carries spin angular momentum (SAM) described as polarization [1] and orbital angular momentum (OAM) associated with helical phase fronts [2]. Compared with SAM, OAM (indexed by l) may increase without bound allowing more information to be packed. The channel capacity available to communication protocols increases concomitantly. Hence, quantum fields based on OAM, such as OAM squeezing and entanglement, have led to many novel insights and applications,

Optics EXPRESS

such as quantum communication [3–7], quantum storage [8], quantum cryptography [9], and quantum metrology [10–12].

Most of the research on OAM quantum states of light has focused on the discrete regime referred to as single-photon or few-photon optics [13–21]. Discrete and continuous-variable systems differ significantly in terms of measurement systems and physical interpretations for quantum entanglement. The CV OAM entanglement is very different to the traditional quadrature entanglement. The generation scheme for CV OAM squeezed and entanglement state was first proposed in 2009 theoretically by Lam and co-workers [22], and then achieved experimentally in a spatially non-degenerate optical parametric oscillator (OPO) by Lassen et al. (2009) [23]. Subsequently, CV hyper-entanglement, with both SAM and OAM states entangled, was proposed theoretically [24] and demonstrated experimentally [25].

Though the CV OAM entanglement has been demonstrated [23, 25], all the previous works were based on balanced homodyne detections to interrogate quadrature entanglement and further to infer the characters of OAM entanglement. The direct measurement and description on Stokes-operator of CV OAM entanglement are essential, and the entanglement of Stokes-operators directly reflect the quantum correlations between OAM light. The more interesting is that the characters of Stokes-operator are related to the rotation of nanoparticle [26] or atoms [27]. With the CV OAM entanglement, the macroscopic entanglement can be generated by the enchantment transfer from light to particles. Additionally, the OAM entanglement with Stokes-operators measurement is more efficient in certain nonlocal quantum information protocols, in which it is hard to select the optimal local oscillators, such as quantum state transmission [28] and quantum key distribution [29].

Here, we report the first direct experimental characterization of a continuous-variable OAM entanglement using the Stokes operator basis. By combining a much more intense HG_{10}-mode coherent beam and a dim HG_{01}-mode-entangled beam produced in a type-II OPO, we achieve continuous-variable OAM entanglement. We verified the OAM entanglement by measuring correlations of the Stokes operators using the scheme described in [30] and quantified the entanglement on the quantum orbital Poincaré sphere.

2. Quantum state of OAM and inseparability criterion

Similar to polarization states [31], the spatial quantum state of a light beam (limited in the first order case) is usually described by a Stokes vector on the Poincaré sphere [22, 32] that is determined by four Stokes operators

$$\hat{O}_0 = \hat{a}_{10}^{\dagger}\hat{a}_{10} + \hat{a}_{01}^{\dagger}\hat{a}_{01} \tag{1a}$$

$$\hat{O}_1 = \hat{a}_{10}^{\dagger}\hat{a}_{10} - \hat{a}_{01}^{\dagger}\hat{a}_{01} \tag{1b}$$

$$\hat{O}_2 = \hat{a}_{10}^{\dagger}\hat{a}_{01}e^{i\theta} + \hat{a}_{01}^{\dagger}\hat{a}_{10}e^{-i\theta} \tag{1c}$$

$$\hat{O}_3 = i\hat{a}_{01}^{\dagger}\hat{a}_{10}e^{-i\theta} - i\hat{a}_{10}^{\dagger}\hat{a}_{01}e^{i\theta} \tag{1d}$$

where $\hat{a}_{10(01)}$ and $\hat{a}_{10(01)}^{\dagger}$ are the annihilation operator and creation operator, respectively, associated with the $HG_{10(01)}$ mode. Operator $\hat{O}_0$ gives the total intensity, whereas $\hat{O}_1$, $\hat{O}_2$, and $\hat{O}_3$ correspond respectively to photon number differences between the HG_{10} and HG_{01} modes, the $+45^o$ and -45^o diagonal HG_{10} modes, and the left and right Laguerre-Gauss modes. The relative phase between the HG_{10} and HG_{01} modes is denoted by θ. The Stokes operators satisfy commutation relations $[\hat{O}_i, \hat{O}_j] = 2i\hat{O}_k$, where $i, j, k \in \{1, 2, 3\}$, their non-commutativity implies that entanglement is possible between the OAM states of two beams.

The photon annihilation operators can be linearized in the form $\hat{a}_{10(01)} = \alpha_{10(01)} + \Delta\hat{a}_{10(01)}$, where $\alpha_{10(01)}$ and $\Delta\hat{a}_{10(01)}$ denote respectively the mean amplitude and quantum noise operator. Assuming that the HG_{01} and HG_{10}-mode light are uncorrelated, the mean amplitudes of the

Optics EXPRESS

Stokes operators and noise variances are therefore given by

$$\langle \hat{O}_0 \rangle = \alpha_{10}^2 + \alpha_{01}^2 \tag{2a}$$
$$\langle \hat{O}_1 \rangle = |\alpha_{10}^2 - \alpha_{01}^2| \tag{2b}$$
$$\langle \hat{O}_2 \rangle = 2\alpha_{10}\alpha_{01}\cos\theta \tag{2c}$$
$$\langle \hat{O}_3 \rangle = 2\alpha_{10}\alpha_{01}\sin\theta \tag{2d}$$

$$\Delta\hat{O}_0 = \alpha_{10}\Delta\hat{X}_{10} + \alpha_{01}\Delta\hat{X}_{01} \tag{3a}$$
$$\Delta\hat{O}_1 = \alpha_{10}\Delta\hat{X}_{10} + \alpha_{01}\Delta\hat{X}_{01} \tag{3b}$$
$$\Delta\hat{O}_2 = \cos\theta(\alpha_{01}\Delta\hat{X}_{10} + \alpha_{10}\Delta\hat{X}_{01}) + \sin\theta(\alpha_{01}\Delta\hat{Y}_{10} + \alpha_{10}\Delta\hat{Y}_{01}) \tag{3c}$$
$$\Delta\hat{O}_2 = \sin\theta(\alpha_{01}\Delta\hat{X}_{10} + \alpha_{10}\Delta\hat{X}_{01}) + \cos\theta(\alpha_{01}\Delta\hat{Y}_{10} + \alpha_{10}\Delta\hat{Y}_{01}) \tag{3d}$$

where $\hat{X}_{10(01)} = \hat{a}_{10(01)} + \hat{a}^{\dagger}_{10(01)}$ and $\hat{Y}_{10(01)} = -i(\hat{a}_{10(01)} - \hat{a}^{\dagger}_{10(01)})$ are the amplitude and phase quadrature operators, respectively, of the $HG_{10(01)}$ mode.

To verify the existence of entanglement, a generalized version of the Duan inseparability criterion is derived. The degree of inseparability is defined in terms of the spatial Stokes vector [22].

$$I(\hat{O}_1, \hat{O}_2) = \frac{\Delta^2_{A\pm B}\hat{O}_1 + \Delta^2_{A\pm B}\hat{O}_2}{8|\alpha_{10}\alpha_{01}\cos\theta|} \tag{4a}$$
$$I(\hat{O}_3, \hat{O}_1) = \frac{\Delta^2_{A\pm B}\hat{O}_1 + \Delta^2_{A\pm B}\hat{O}_3}{8|\alpha_{10}\alpha_{01}\cos\theta|} \tag{4b}$$
$$I(\hat{O}_2, \hat{O}_3) = \frac{\Delta^2_{A\pm B}\hat{O}_2 + \Delta^2_{A\pm B}\hat{O}_3}{4|\alpha_{10}^2 - \alpha_{01}^2|} \tag{4c}$$

where $\Delta^2_{A\pm B}\hat{O}_i$ is the smaller of correlation variances of the operator $\hat{O}_i$ between between beam A ($Alice$) and B (Bob) and given by $\Delta^2_{A\pm B}\hat{O}_i = min\langle(\Delta\hat{O}_i^A \pm \Delta\hat{O}_i^B)^2\rangle$ [22]. If $I(\hat{O}_i, \hat{O}_j) < 1$, the state is said to be inseparable and therefore entangled for the pair of optical beams associated with Stokes operators $\hat{O}_i$ and $\hat{O}_j$. Substituting Eq. (3) into Eq. (4), gives the expression in terms of quadrature operators

$$\begin{aligned} I(\hat{O}_1, \hat{O}_2) &= \frac{\alpha_{10}}{8\alpha_{01}|\sin\theta|}(\Delta^2_{A\pm B}\hat{X}_{10} + \Delta^2_{A\pm B}\hat{X}_{01}\cos^2\theta + \Delta^2_{A\mp B}\hat{Y}_{01}\sin^2\theta) \\ &\quad + \frac{\alpha_{01}}{8\alpha_{10}|\sin\theta|}(\Delta^2_{A\pm B}\hat{X}_{01} + \Delta^2_{A\pm B}\hat{X}_{10}\cos^2\theta + \Delta^2_{A\mp B}\hat{Y}_{10}\sin^2\theta) \end{aligned} \tag{5a}$$
$$\begin{aligned} I(\hat{O}_3, \hat{O}_1) &= \frac{\alpha_{10}}{8\alpha_{01}|\cos\theta|}(\Delta^2_{A\pm B}\hat{X}_{10} + \Delta^2_{A\pm B}\hat{X}_{01}\sin^2\theta + \Delta^2_{A\mp B}\hat{Y}_{01}\cos^2\theta) \\ &\quad + \frac{\alpha_{01}}{8\alpha_{10}|\cos\theta|}(\Delta^2_{A\pm B}\hat{X}_{01} + \Delta^2_{A\pm B}\hat{X}_{10}\sin^2\theta + \Delta^2_{A\mp B}\hat{Y}_{10}\cos^2\theta) \end{aligned} \tag{5b}$$
$$I(\hat{O}_2, \hat{O}_3) = \frac{\alpha_{10}^2(\Delta^2_{A\pm B}\hat{X}_{01} + \Delta^2_{A\mp B}\hat{Y}_{01}) + \alpha_{01}^2(\Delta^2_{A\pm B}\hat{X}_{10} + \Delta^2_{A\mp B}\hat{Y}_{10})}{4|\alpha_{10}^2 - \alpha_{01}^2|} \tag{5c}$$

From Eq. (5), we see that the OAM entanglement can be achieved by combining HG_{01} and HG_{10} mode quadrature entangled states and the degree of OAM entanglement dependents on the amplitude ratio (α_{10}/α_{01}) and the relative phase θ between HG_{01} and HG_{10} modes. As shown in the Fig.1, we plot the degree of inseparability, and here the HG_{01} and HG_{10} mode are 10 dB entanglement.

Optics EXPRESS

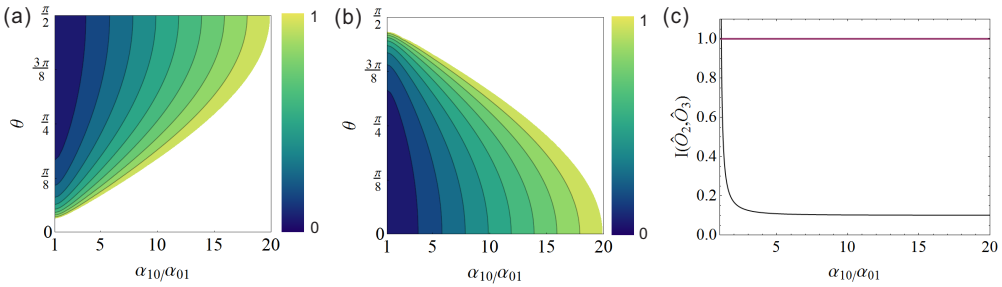

Fig. 1. The degree of inseparability for (a)$I(\hat{O}_1,\hat{O}_2)$, (b)$I(\hat{O}_3,\hat{O}_1)$ and (c)$I(\hat{O}_2,\hat{O}_3)$ as a function of the amplitude ratio (α_{10}/α_{01}) and the relative phase θ between HG_{01} and HG_{10} modes.

In Fig. 1(a) and (b) OAM entanglement exists in the non-white region, where the values of I are below unity (the bound of inseparability). The degree of inseparability for $I(\hat{O}_1,\hat{O}_2)$ (Fig.1(a)) will degrade and even disappear as α_{10}/α_{01} increases but θ decreases, the maximum entanglement between $\hat{O}_1$ and $\hat{O}_2$ is achieved when $\theta=\frac{\pi}{2}$ & $\alpha_{10}/\alpha_{01}=1$. The degree of inseparability for $I(\hat{O}_3,\hat{O}_1)$ (Fig.1(b)) will degrade and even disappear as θ and α_{10}/α_{01} increase, the maximum entanglement between $\hat{O}_3$ and $\hat{O}_1$ is achieved when $\theta=0$ & $\alpha_{10}/\alpha_{01}=1$.

According to the Eq. 5(c), $I(\hat{O}_2,\hat{O}_3)$ is independent on the relative phase θ. The Fig. 1(c) shows the relationship of the $I(\hat{O}_2,\hat{O}_3)$ vs α_{10}/α_{01}. We can find that the OAM entanglement between $\hat{O}_2$ and $\hat{O}_3$ increases with α_{10}/α_{01} increasing, and when $\alpha_{10}/\alpha_{01}\gg 1$, the entanglement reaches the maximum value. The condition $\alpha_{10}/\alpha_{01}\gg 1$ indicates that we can replace the HG_{10} entanglement with a bright coherent light in HG_{10} mode to generate the optimal OAM entanglement with Stokes operators $\hat{O}_2$ and $\hat{O}_3$.

Therefore, by spatial overlapping two quadrature entanglement in HG_{01} and HG_{10} mode with equal power, and controlling their relative phase between HG_{01} and HG_{10} mode to $\frac{\pi}{2}$ or 0, the maximum entanglement with Stokes operators $\hat{O}_1$ and $\hat{O}_2$ or $\hat{O}_3$ and $\hat{O}_1$ can be achieved respectively. The maximum entanglement with $\hat{O}_2$ and $\hat{O}_3$ can be generated by combing bright coherent beams in HG_{10} mode and entanglement in HG_{01} mode.

Here we focus on the experimental generation of the OAM entanglement associated with Stokes operators $\hat{O}_2$ and $\hat{O}_3$. In more intuitive picture, the OAM state is related to the rotation of photons around the propagation direction of light [12], the $\hat{O}_2$ refers to the rotational angular position and $\hat{O}_3$ refers to the rotation angular momentum. The type of OAM entanglement is more useful into rotational optomechanics by interacting with nanoparticle to realize high-precision angular measurement for future quantum gyroscopes and even demonstrate the macroscopic entanglement.

3. Experimental set-up and results

The experimental setup (Fig. 2) to generate and characterize OAM-state entanglement, comprises (a) HG_{01}-mode entanglement-source creation and quadrature entanglement detections, and (b) OAM entanglement generation and Stokes-operator measurement.

The optical parametric amplifier (OPA) cavity is composed of two plano-concave mirrors, each with radius of curvature of 30 mm. The nonlinear medium, a type-II KTP crystal, is placed in the center of the cavity. The input mirror is coated to give high reflectivity at both 1080 nm and 540 nm, whereas the output coupler has a transmittance of 6% at 1080 nm, and a high transmittance at 540 nm. The OPA is seeded with dim 1080-nm HG_{01} light, enabling active cavity locking, and pumped with 540-nm HG_{02} light, therefore having higher pump efficiency than the HG_{00} mode [33, 34]. When we lock the relative phase between the pump field and the injected

Optics EXPRESS

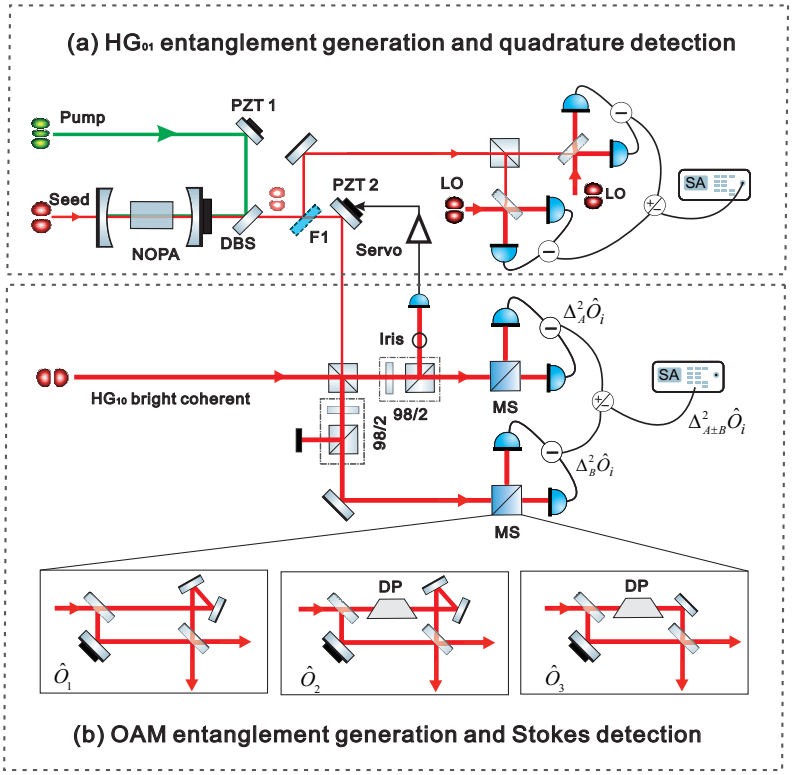

Fig. 2. Experimental generation and characterization of entanglement of first-order OAM modes. The entanglement source, specifically, (a) HG_{01} mode quadrature and (b) OAM state entanglement, are measured in quadrature detection and Stokes detection, respectively. DBS: dichroic beam splitter; F1: flip mirrors; PBS: polarizing beam splitter; MS: measuring system; DP: Dove prism; SA: spectrum analyzer.

seed beam in the state of deamplification with PZT1, The HG_{01}-mode quadrature entanglement between two down-converted fields in orthogonal linear polarizations is generated and separated from the pump light using a dichroic beam splitter. When F1 is present, the output entangled beams are divided by the polarizing beam splitter into two parts and sent into balanced homodyne detections with a HG_{01}-mode local oscillator to perform the quadrature measurements.

When F1 is off, the HG_{01}-mode entangled beams and a bright HG_{10} coherent beam in 45^o polarization are coupled on PBS and divided into two parts. Each part including a bright beam in HG_{10}-mode and an entangled beam in HG_{01}-mode, is sent into 98/2 beam splitter which consists of a half-wave plate and a polarization beam splitter to ensure that the entangled beams of 98% are transmitted and the coherent beams of 2% are reflected. By the way, the lossless coupling between HG_{01} mode and HG_{10} mode can be realized with the help of an asymmetric Mach-Zehnder interferometer [22]. As a result, the components of HG_{01} and HG_{10} mode of output from 98/2 beam splitter are in the same polarization and their powers satisfy $\alpha_{10}^2 = 30\alpha_{01}^2$. In order to generate the OAM entanglement, the coupling of HG_{01} mode and HG_{10} mode requires mode matching and phase locking. Although there is no interference between the two spatial orthogonal modes, the relative phase can be monitored from part of the interference by a detector with an aperture (marked Iris in Fig. 2) and controlled to be 0 with PZT2.

The OAM entanglement beams produced are sent to a measuring system (MS) comprising an asymmetric/symmetric Mach−Zehnder interferometer and a Dove prism. Depending on their

Optics EXPRESS

different combinations, the resulting difference in photocurrent between the two photodiodes yields instantaneous values for $\hat{O}_1$, $\hat{O}_2$ or $\hat{O}_3$, and the sum photocurrent yields the corresponding limits of quantum noise, see details in [30]. The measured Stokes parameters of the two entangled beams are summed/subtracted and finally sent to a spectrum analyzer to characterize their correlations.

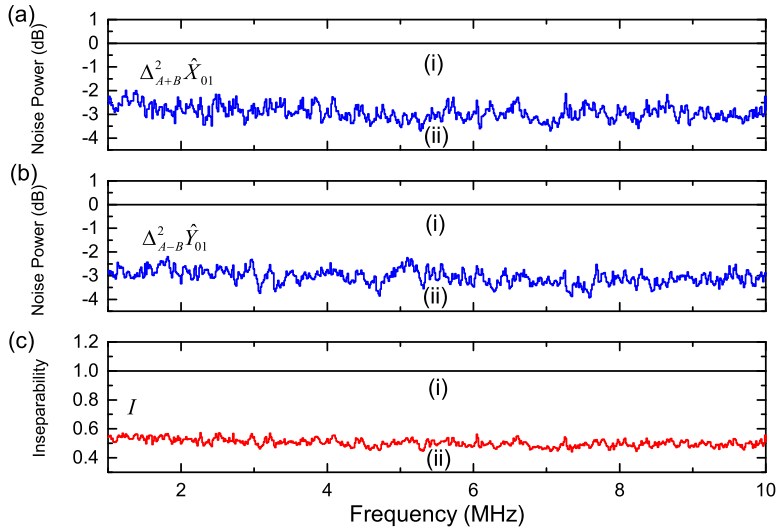

Fig. 3. Correlation variance measurements of the HG_{01}-mode entangled beam for (a) quadrature amplitude sum $\Delta^2_{A+B}\hat{X}_{01}$, (b) phase difference $\Delta^2_{A-B}\hat{Y}_{01}$, and (c) degree of inseparability. In (a) and (b), trace (i) is the SNL and trace (ii) the correlation variance normalized to SNL. In (3), trace (i) is the bound of inseparability (unity), and trace (ii) degree of inseparability. All data are normalized with respect to shot-noise level. The measurement parameters of spectrum analyzer: RBW=300 kHz, VBW=200 Hz.

From the measured correlation variance of the HG_{01} mode entangled beam (Fig. 3), traces (i) in (a) and (b) are the corresponding shot-noise levels, obtained by blocking the entangled beam. The correlation variances of the amplitude sum $\Delta^2_{A+B}\hat{X}_{01}$ [trace (ii) in (a)] and the phase difference $\Delta^2_{A-B}\hat{Y}_{01}$ [trace (ii) in (b)] between the output signal and idler fields are all more than 2.5 dB below the shot-noise level in the range of frequencies from 1 to 10 MHz. This implies that non-classical correlations exist between the two beams. From 4–7 MHz, we observe optimal results with mean values of 2.70±0.18 dB and 2.75±0.12 dB for the amplitude sum and phase difference, respectively. Taking the sum of the amplitude sum and phase difference quadrature variances yields the degree of inseparability of 0.53±0.02 [Fig. 3(c)], which is well below the bound of inseparability (unity), indicating the state is inseparable and entangled. All data are normalized using the level of shot noise. The total detection efficiency is 75 %.

From the measured variance spectra of the Stoke operator (a) $\Delta^2_{A\pm B}\hat{O}_2$ and (b) $\Delta^2_{A\pm B}\hat{O}_3$ (Fig. 4), traces (ii) and (iii) are the corresponding anti-correlation and correlation variance, respectively. We find that the correlation variance for both $\Delta^2_{A+B}\hat{O}_2$ and $\Delta^2_{A-B}\hat{O}_3$ are more than 1.5 dB below shot-noise levels [trace (i)] over the range of measurements. From 4–7 MHz, we obtain optimal correlation variances with mean values of 1.8±0.10 dB and 1.8±0.12 dB for $\Delta^2_{A+B}\hat{O}_2$ and $\Delta^2_{A-B}\hat{O}_3$, respectively. All data are normalized with respect to shot-noise levels. Notice that the correlation variance for $\Delta^2_{A+B}\hat{O}_2$ and $\Delta^2_{A-B}\hat{O}_3$ is degraded compared with the inferred value from quadrature entanglement because of losses mainly resulting from the polarization-impurity induced by the Dove prism and added optical elements. The peaks around 4 MHz in trace (ii) result from the coupling of residual modulation signal that is used to lock the cavity.

Optics EXPRESS

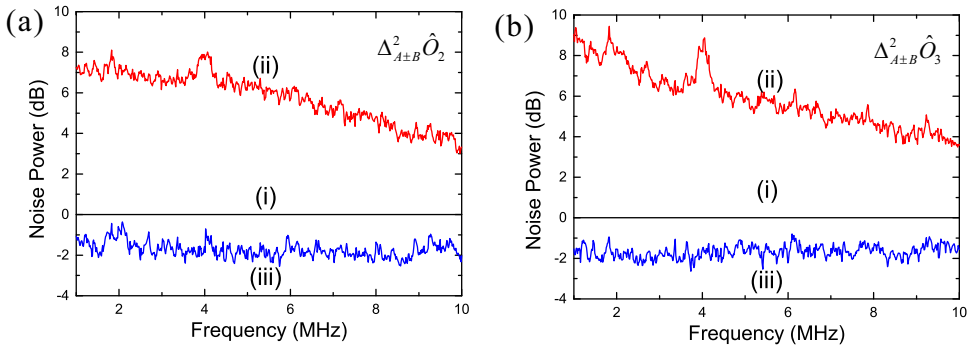

Fig. 4. Measured variance spectra of quantum noise on (a)$\Delta^2_{A\pm B}\hat{O}_2$ and (b)$\Delta^2_{A\pm B}\hat{O}_3$ for OAM entangled beams. In (a) and (b), trace (i) is the SNL, trace (ii) the correlation variance and trace (iii) the anti-correlation variance normalized to SNL. All data are normalized with respect to shot noise level. The measurement parameters of the spectral analyzer: RBW=300 kHz, VBW=200 Hz.

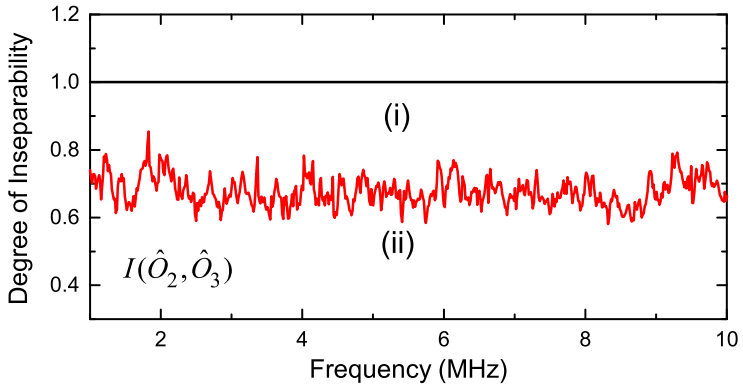

Fig. 5. Experimental measurement of $I(\hat{O}_2, \hat{O}_3)$ at Fourier frequencies from 1 to 10 MHz. Trace (i) is the bound of inseparability (unity), and trace (ii) degree of inseparability. Values below unity indicate entanglement.

By substituting correlation variance of $\Delta^2_{A+B}\hat{O}_2$ and $\Delta^2_{A-B}\hat{O}_3$ into the entanglement criterion, we obtain the degree of inseparability $I(\hat{O}_2, \hat{O}_3)$ [Fig. 5]. Traces (ii) are below unity [traces (i)] over almost the entire measurement range, indicating that the OAM entanglement exists for Stokes operators $\hat{O}_2$ and $\hat{O}_3$. From 4–7 MHz, we obtain an optimum of $I(\hat{O}_2, \hat{O}_3) = 0.66 \pm 0.03$.

Figure 6 presents a visualization of the experimental fluctuations at 5.0 MHz on the orbital Poincaré sphere; panel (a) gives its location because the mean value identifies the HG_{10} mode, and (b) presents information carried by beam A, which is the same result as beam B, without any measurement; all measurements of the three Stokes operators are above the quantum noise limit. Panels (c) and (d) show respectively the conditional knowledge of beam A given correlation variance measurements of Stokes operators $\hat{O}_2$ and $\hat{O}_3$ on beam B. Thus the value of the Stokes operator on beam A becomes known to an accuracy better than the quantum noise limit upon measurement.

4. Summary

We have described the experimental generation and characterization of continuous-variable first-order OAM entanglement. The generation scheme entails transforming HG_{01}-mode entanglement

Optics EXPRESS

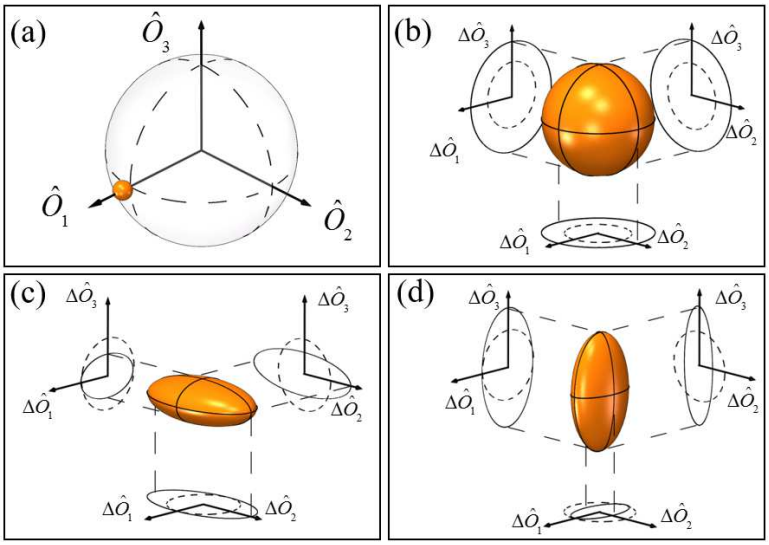

Fig. 6. Entanglement descriptions mapped onto quantum orbital Poincaré spheres at 5.0 MHz. (a) Location of output beams on the orbital Poincaré sphere. (b) Knowledge of beam A before any measurement of beam B. (c) Conditional knowledge of beam A after measurements of $\hat{O}_2$ on beam B. (d) Conditional knowledge of beam A after measurements of $\hat{O}_3$ on beam B. The dashed circles define the classical correlation limit, and conditional knowledge outside the dashed circles indicates entanglement.

to OAM entanglement. The measurements were conducted in the Stokes operators basis with a local oscillator-free homodyne detection scheme. The results demonstrate that OAM entanglement is present for the Stokes-operator pair $\hat{O}_2$ and $\hat{O}_3$. We also presented our results using a quantum version of the orbital Poincaré sphere representation.

Such OAM entanglement, due to more degrees of freedom than quadrature entanglement, offers a very large state space to encode and manipulate quantum information, which holds the great potential in high-dimensional quantum information processing, such as the CV quantum key distribution (QKD), quantum dense coding protocols [35–37]. Especially, the CV OAM states with a local oscillator-free homodyne detection scheme, lead to some nonlocal applications where the local optimal local oscillators is hard to generate. This enables the measurements [10, 11] and communications [28, 29] to be done remotely and efficiently. Moreover, it is conceivable that the state could be used into rotational optomechanics involving interaction with nanoparticle to realize high-precision angular measurement for future quantum gyroscopes and even demonstrate the macroscopic entanglement of micro-organism [38].

Funding

National Key R & D Program of China (2016YFA0301404); National Natural Science Foundation of China (NSFC) (91536222, 11674205); Program for Outstanding Innovative Team of Higher Learning Institution of Shanxi and Shanxi (1331 Project).